DOI 10.1007/s11106-021-00190-9
Powder Metallurgy and Metal Ceramics, Vol. 59, Nos. 9-10, January, 2021 (Russian Original Vol. 59, Nos. 9-10, Sept.-Oct., 2020)

SINTERED METALS AND ALLOYS

STRUCTURAL AND ELECTRICAL PROPERTIES OF MAGNESIUM-DOPED $CoFe_2O_4$

D. Mohanty,[1] A.U. Naik,[2] P.K. Nayak,[1]
Banarji Behera,[2] and S.K. Satpathy[1,3]

UDC 537.226;669.7

In this paper, magnesium-doped $CoFe_2O_4$ ($Co_{0.5}Mg_{0.5}Fe_2O_4$) compound was synthesized by a solid-state reaction route. The impact of Mg inclusion on the structural parameters of the obtained compound and the subsequent development of thermally-assisted electro-active areas has been systematically examined, as this compound has a fit composition for doping at the site of Co due to its relevantly equal atomic radius. Also, Mg was established as highly ferroelectric and low-weight material. The compound structure and microstructure have been analyzed using the method of scanning electron microscopy (SEM) and X-ray diffraction (XRD) analysis. The dielectric properties were studied over a broad spectrum of frequency and temperature, and quite low dielectric loss was recorded. In the context of impedance and conductivity formalism, frequency-dependent electrical information has been evaluated at varying temperatures. The Nyquist plot represents the effect of grain and grain boundary. Thermally activated non-Debye type relaxation processes were observed in the composites. Jonscher universal power law follows the frequency-dependent AC conductivity at different temperatures. Temperature dependence of AC conductivity at various frequencies indicates a negative temperature coefficient of resistance (NTCR) behavior. Estimating the magnitudes of activation energies in different temperature ranges enables defining the nature of the species involved in the conduction system.

Keywords: *dielectric constant, SEM, XRD, Nyquist plot, activation energy.*

INTRODUCTION

In recent years, spinel ferrites have been extensively studied owing to their outstanding electrical and magnetic characteristics, which allows for wide applications range in systems of information storage, sensors, telecommunications devices, microwave absorbers, etc. [1]. Therefore, great attention has been given to the synthesis and characterization of spinel ferrite nanoparticles.

Many scientists have performed extensive research on the structural and magnetic characterization of nano-sized spinal ferrites [2]. Due to their mechanical hardness, mild saturation magnetization, elevated electrical

[1]Centurion University of Technology and Management, Odisha, India. [2]Materials Research Laboratory, School of Physics, Sambalpur University, JyotiVihar, Burla, 768019, Odisha, India.

[3]To whom correspondence should be addressed; e-mail: santosh.satpathy@cutm.ac.in.

Published in Poroshkova Metallurgiya, Vol. 59, Nos. 9–10 (535), pp. 32–40, 2020. Original article submitted October 17, 2019.

characteristics, elevated magneto-crystalline anisotropy, thermal stability, elevated magnetostriction coefficient, big coercive field, and anisotropy coefficient, cobalt ferrites with reverse spinel structure are very promising material among other ferrites [3–5]. Also, cobalt ferrites are very favourable for applications in electronics for magnetic stress sensors, gas sensors, and high-density information storage systems due to these notable characteristics [6–8]. Magnesium (Mg^{2+}) is considered a non-magnetic object when the structural and magnetic characteristics are altered by the solid-state response technique in cobalt ferrite [9, 10].

The objective of this study is, therefore, to synthesize Mg^{2+} cobalt ferrite by the solid-state reaction technique and examine the structural and electrical characteristics of the resulted compound. Recently, the investigation of the temperature-dependent dielectric properties of Mg-doped $CoFe_2O_4$ nanoparticles revealed a fast rise in dielectric constant and dielectric loss with an increase in temperature.

The emphasis of the current study is to systematically examine the impact of Mg inclusion on the structural parameters at the Co-site, i.e., $Co_{0.5}Mg_{0.5}Fe_2O_4$ and the subsequent development of thermally-assisted electro-active areas, as this compound has a fit composition for doping at the site of Co due to its relevantly equal atomic radius. Also, Mg is highly ferroelectric and low-weight material.

EXPERIMENTAL PROCEDURE

The sample of Mg-doped $CoFe_2O_4$ ($Co_{0.5}Mg_{0.5}Fe_2O_4$) was prepared by high-temperature solid-state reaction technique using high-purity stoichiometry ingredients. The material weighed stoichiometrically was carefully ground, first for 2 h in an air atmosphere and then for another 1 h in alcohol. Afterward, the mixed powders were calcined at an optimized temperature of 950°C for 4 h in an alumina crucible of high purity (air media).

The compound formation was verified using the method of X-ray diffraction (Rigaku, Ultima IV). Calcined powders were then ground with polyvinyl alcohol (PVA) to produce the pellet. The fine homogeneous powders were cold-pressed into a cylindrical pellet of $3 \cdot 10^6$ N/m^2 using a hydraulic press. Next, these pellets were sintered at 1000°C in an air atmosphere for 4 h. Finally, the sintered pellets were polished with the emery paper to make both surfaces smooth and parallel.

For electrical measurements, the pellet faces were coated with a silver paste of high purity and dried at 100°C. Dielectric and impedance measurements were performed using an LCR meter (Impedance Analyzer, IM 3570).

RESULTS AND DISCUSSION

Structural and Dielectric Study. The room temperature of Mg-doped cobalt ferrite ($Co_{0.5}Mg_{0.5}Fe_2O_4$) is shown on the XRD pattern in Fig. 1. The X-ray diffraction analysis confirmed the Cubic Spinel Structure with a lattice parameter of a = 0.840 nm [11]. The chosen unit cells' grid parameters are refined using a conventional 'POWD' computer program package [12]. A strong agreement has been established found between observed (obs) and calculated (cal) interplanar spacing and is well aligned with interplanar spacing ($\Sigma\Delta d = d_{obs} - d_{cal}$ = minimum). The crystallite size is roughly estimated from the expansion of XRD peaks (two wide ranges) using Scherer's

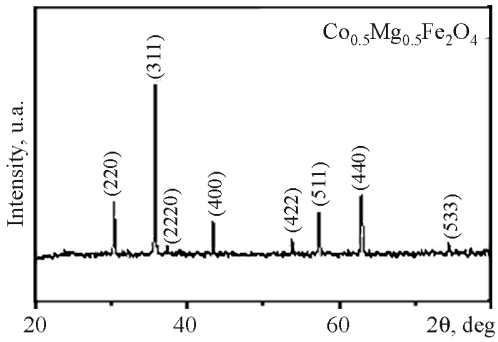

Fig. 1. XRD pattern of $Co_{0.5}Mg_{0.5}Fe_2O_4$ at room temperature

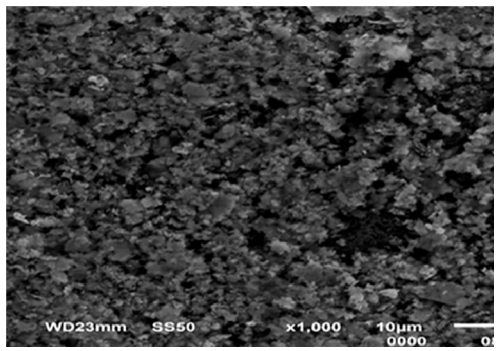

Fig. 2. SEM images of $Co_{0.5}Mg_{0.5}Fe_2O_4$ at room temperature

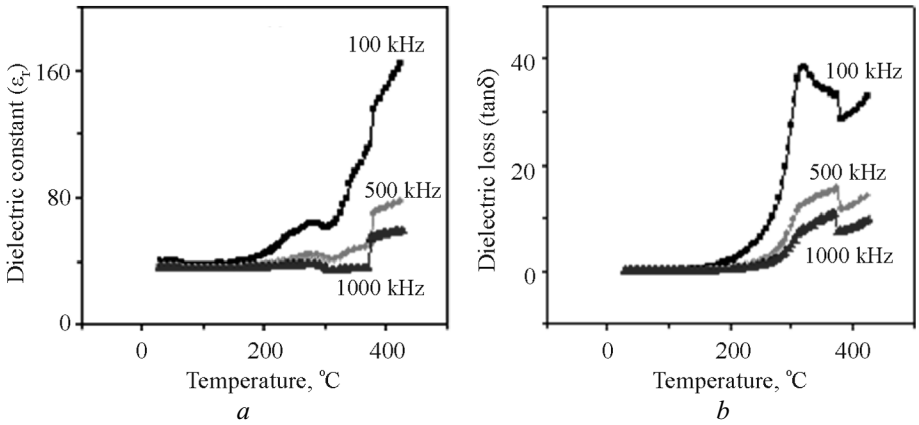

Fig. 3. Temperature dependence variation of ε_r (*a*) and tanδ (*b*) of $Co_{0.5}Mg_{0.5}Fe_2O_4$

equation [13]: $P = K\lambda/((\beta_{(1/2)} \cdot \cos\theta_{hkl})$, where K is a constant ($K = 0.89$), $\lambda = 0.1540(5)$ nm, and $\beta_{(1/2)}$ is the peak width of the reflection at half intensity. The average crystallite size (P) is 29 nm.

Figure 2 represents the scanning electron microscope image of $Co_{0.5}Mg_{0.5}Fe_2O_4$. The method of scanning electron microscopy (SEM) is very helpful for thorough research of the specimen surface. The interactions between the sample and the electron beam resulted in distinct types of electron signals being emitted during the scanning. The grains are spread more or less homogeneously with less porosity throughout the sample surface. The shape of the grains is spherical. The average size of the grain is 10 μm. It has been noted that the size of the grain is greater than the size of the crystallite acquired from Scherer's equation. Thus, several crystallites can consist of a single grain.

Figures 3 show the variation of ε_r and tanδ with the temperature at different frequencies. It shows that the dielectric constant (ε_r) increases with an increase in temperature [14]. Besides, a dielectric anomaly is noted at higher temperatures. The dielectric constant variation relies on the alignment of the domain and these results in an increase in the dielectric constant. The tanδ values decreased with the rise in temperature [15], which can be due to the improvement of electrical conductivity.

Impedance Properties. The complex impedance analysis [16] is quite a well-known and powerful tool for investigating the material's electrical (i.e., transportation) properties at a wide frequency range. This technique helps to measure the real and imaginary components of complex electrical parameters like impedance, modulus, etc.

Figure 4*a* shows the variation of real impedance (Z') on the frequency of $Co_{0.5}Mg_{0.5}Fe_2O_4$ at different temperatures. The entire curve merges in one frequency region at the high-frequency area, which may be due to the

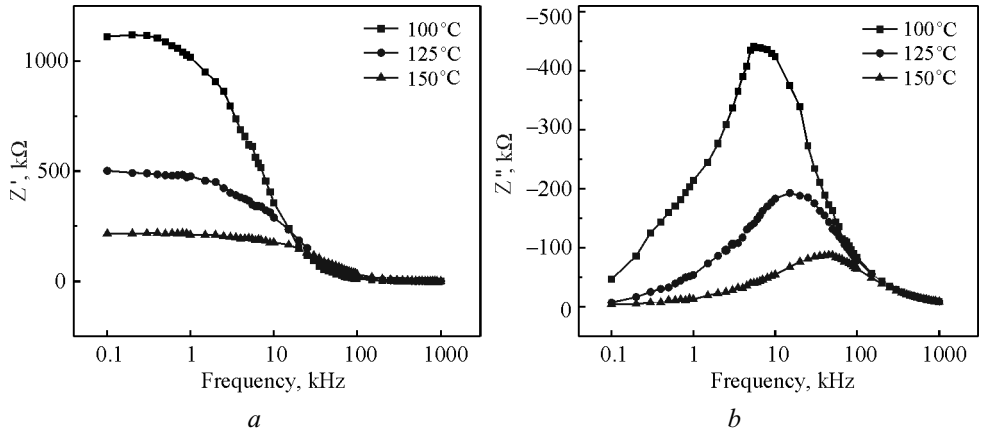

Fig. 4. Variation of real (*a*) and visionary (*b*) parts of impedance as a function of $Co_{0.5}Mg_{0.5}Fe_2O_4$ frequency at different temperatures

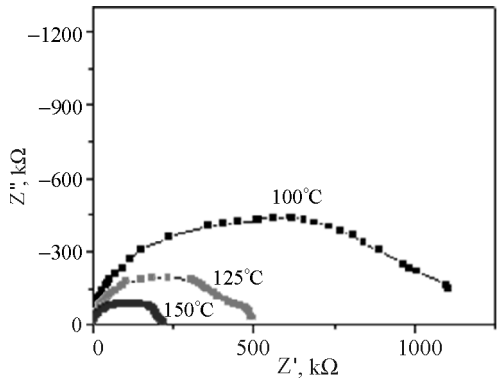

Fig. 5. Variation between Z' and Z" of $Co_{0.5}Mg_{0.5}Fe_2O_4$ at different temperatures

TABLE 1. Calculation of Bulk Resistance and Grain Boundary Resistance at Different Temperatures Following Nyquist Plot

Temperature, °C	R_b, kΩ	R_{gb}, kΩ
200	14.118	4.436
225	14.024	4.214
250	7.328	1.645

release of space charges polarization with increasing frequency [17]. The magnitude of Z' is observed to decrease with the rise in temperature, which shows a negative temperature coefficient of resistance (NTCR) behavior [18].

Figure 4*b* shows the frequency dependence of Z" on the frequency of $Co_{0.5}Mg_{0.5}Fe_2O_4$ at different temperatures. Thus, the plot peak is moved to a greater frequencies side with an increase in temperature. The peak widening changes with temperature variations indicate the presence of relaxation processes depending on the temperature in the material, which can be attributed to the existence of immobile species and greater deficiencies at low temperature [19]. The maximum width of the loss spectrum displays relaxation time distribution. The maximum expansion and asymmetric spectrum suggest the relaxation method in the material to be of non-Debye type. The bulk resistance and grain boundary resistance decrease with the temperatures rise (Table 1).

The variation between Z' and Z" values of the $Co_{0.5}Mg_{0.5}Fe_2O_4$ compound at selected temperatures is demonstrated in Fig. 5. This figure shows that the material electrical characteristics occur due to the contribution of grain as well as grain boundary effects. It also shows that the intercept point on the real axis changes the origin with the temperature increase, suggesting a decrease in the resistive property of the material [20]. It provides the materials with the bulk (R_b) and grain boundary (R_{gb}) resistance.

The complex electrical modulus formalism was introduced to study the suppressed electrode polarization effects and for a better insight into the electric relaxation. Figure 6*a* depicts the real (M') parts of electric modulus data plotted against the frequency of the $Co_{0.5}Mg_{0.5}Fe_2O_4$ compound. Real modulus M' approaches to zero at low frequency, and the existence of a long tail may be due to the impact of electrode polarization connected with the high double-layer capacitance. An asymmetric maximum is achieved at a greater frequency that confirms the presence of space charge polarization phenomenon [20].

When the frequency increases, the dispersion is noticed and saturation is reached at the very high values in the real part of the modulus. A continuous dispersion on increasing frequency may be contributed to the conduction phenomena due to the short-range mobility of charge carriers [21].

The variation of M" with $Co_{0.5}Mg_{0.5}Fe_2O_4$ frequency at different temperatures is shown in Fig. 6*b*. The M" value rises to a peak and then decreases as the frequency goes low. The frequency at which M" reaches a maximum is called the frequency of relaxation. The M'_{max} peak shifts with temperature increase to the higher frequency side.

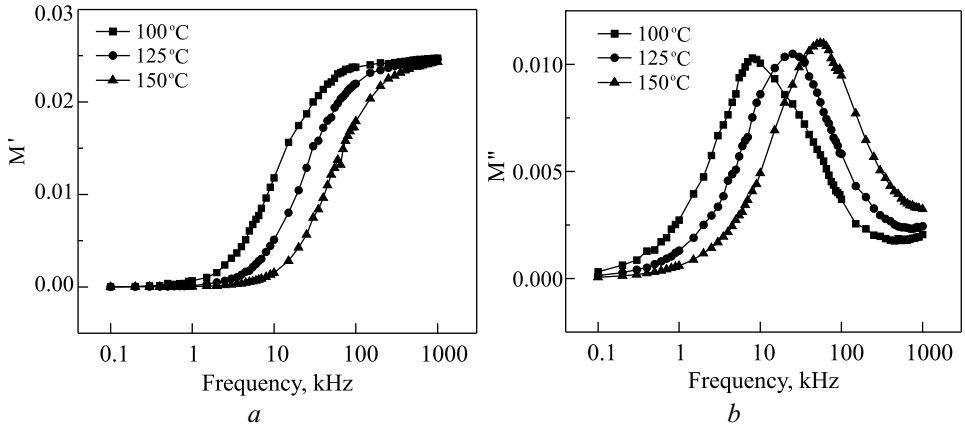

Fig. 6. Variation of M' (*a*) and M" (*b*) with frequency of $Co_{0.5}Mg_{0.5}Fe_2O_4$ at different temperatures

This behavior confirms the presence of relaxation involvement in the materials. It is noted that the temperature reliance of asymmetric peak expansion confirms the spread of relaxation with distinct time constants. Hence, the relaxation in the material is considered to be of non-Debye type [22].

The scaling behavior of $Co_{0.5}Mg_{0.5}Fe_2O_4$ is studied by plotting Z''/Z''_{max} and M''/M''_{max} against frequency at selected temperatures (100–150°C) (Fig. 7). Normally, these plots are used to detect the existence of the lowest capacity and the greatest resistance proposed by Sinclair et al. [23], which will assist to define the relaxation method whether charging carriers have a brief variety or lengthy range movement. The low-frequency part of the peak in the M''/M''_{max} vs frequency curves is the range in which the charging carriers can move over a long distance. The charging carriers are confined spatially to their potential wells within the high-frequency range and could thus make localized motions within the well. The region of the peak occurrence is an indication of the long-range shift to short-range mobility with increased frequency [24].

Conductivity Examination. The frequency dependence of AC conductivity in $Co_{0.5}Mg_{0.5}Fe_2O_4$ at different temperatures is shown in Fig. 8. Based on the dielectric information, the AC conductivity was assessed using the relationship $\sigma_{ac} = \omega\varepsilon_0\varepsilon_r\tan\delta$. All AC conductivity graphs are well suited to the Johns Cher's power-law [25], and solid lines represent the fitted curves. The solid lines in the AC conductivity spectra denote the fit of exponential data to the power law expression: $\sigma_{ac} = \sigma_0 + A\omega^n$, where A is a parameter which has the conductivity unit, n is a dimensionless parameter, and ω is the angular frequency at which the AC conductivity σ_{ac} was measured. The

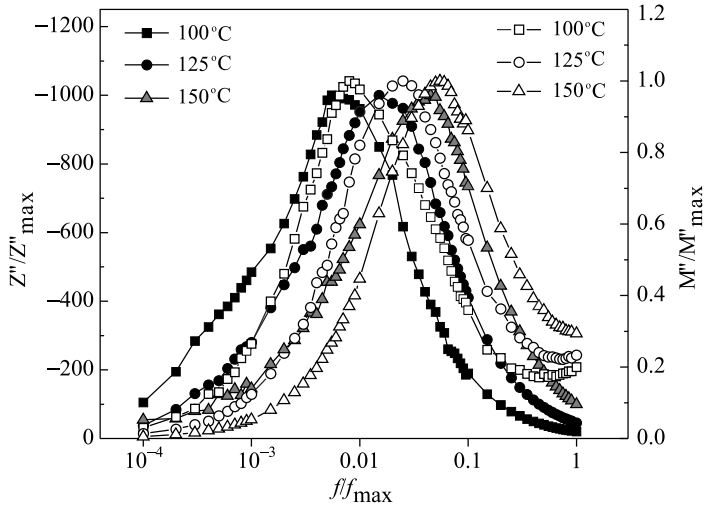

Fig. 7. Variation of Z''/Z''_{max} and M''/M''_{max} with $\log f/f_{max}$ of $Co_{0.5}Mg_{0.5}Fe_2O_4$ at different temperatures

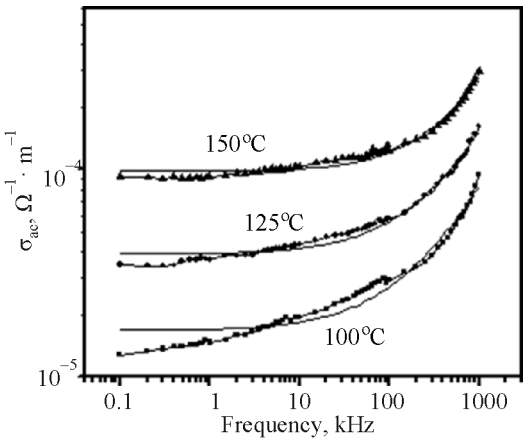

Fig. 8. Variation of σ_{ac} as a function of frequency in $Co_{0.5}Mg_{0.5}Fe_2O_4$ at different temperatures

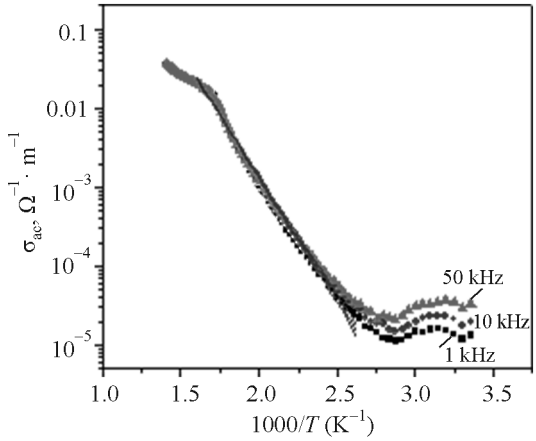

Fig. 9. Variation of AC electrical conductivity (σ_{ac}) with inverse of $Co_{0.5}Mg_{0.5}Fe_2O_4$ temperature

TABLE 2. Fitting Parameters Following the Jonscher Power Law at Different Temperatures

T, °C	σ_{dc}, $\Omega^{-1} \cdot m^{-1}$	A	n
100	$1.676 \cdot 10^{-5}$	$1.0622 \cdot 10^{-9}$	0.79888
125	$3.91825 \cdot 10^{-5}$	$1.4107 \cdot 10^{-9}$	0.81682
150	$9.83904 \cdot 10^{-5}$	$6.09814 \cdot 10^{-10}$	0.91291

temperature variation of n indicates the conductive mechanism type in the material [21]. The AC conductivity spectrum shows that the material systematically shows a steadily growing trend towards growing frequency.

However, a frequency-independent plateau-like area appears in the low-frequency spectrum as a comparative assessment of conductivity spectra, and consequently, the nature of AC conductivity rises with an increase in frequency. The value n is noted to increase linearly with a temperature of 100–150°C, which may be the consequence of the increase in electrode polarization with temperatures at all levels.

The value n is less than 1 for the translation motion, whereas the value of localized n is more than 1 [26]. If $n < 1$, charge carriers take a translational motion with a sudden hopping, while $n > 1$ would mean a localized hopping of the species (small hopping without leaving the neighborhood), and at $n = 1$ they behave like ideal capacitors [27]. Figure 8 shows that n is temperature-dependent, decreasing with an increase in temperature, which follows the small polaron model given in Table 2.

Figure 9 shows the variation of σ_{ac} (bulk) with the inverse of absolute temperature 10^3/T (K^{-1}) for $Co_{0.5}Mg_{0.5}Fe_2O_4$. As can be seen, the AC conductivity is found to be higher with the temperature rise. At high temperature, σ_{ac} of the different frequency merges. Hence, the frequency-independent nature corresponds to DC conductivity in that region. The activation energy of Mg doped $CoFe_2O_4$ decreases with growing frequency within a temperature range of 50–150°C: E_a = 0.63, 0.61, and 0.60 eV at frequency of 1, 10, and 50 kHz, respectively. Thus, the activation energy is the total of energy engaged in generating charge carriers, but for polycrystalline-like products, the faults at greater temperatures can provide extra acceptor centers, which means that the process is thermally activated.

CONCLUSIONS

The polycrystalline $Co_{0.5}Mg_{0.5}Fe_2O_4$ sample was prepared by a solid-state reaction method at high temperature. The preliminary structural analysis confirmed the formation of the material with a cubic spinel

structure at room temperature. The material exhibited a dielectric anomaly at high-temperature values. It has been established that the average grain sizes are within the range of 10 μm, which confirmed that the grains were bigger than the average crystallite sample. The Nyquist plot revealed the bulk and grain boundary effects in the materials. The AC conductivity study with frequency obeys the power law of the form $\sigma_{ac} = \sigma_0 + A\omega^n$, with n found to be in the range 0.79–0.92. The AC conductivity acquired from dielectric information exhibited electrical conductivity of the Arrhenius type and the value of E_a reduces as temperatures rise.

REFERENCES

1. Ra'ul Valenzuela, "Novel applications of ferrites," *Phys. Research Int.*, **2021**, 1–9 (2011).
2. Vithal Vinayak, Pankaj P. Khirade, Shankar D. Birajdar, P.K. Gaikwad, N.D. Shinde, and K.M. Jadhav, "Low temperature synthesis of magnesium doped cobalt ferrite nanoparticles and their structural properties," *Int. Adv. Research J. Sci., Eng. Technol.*, **2**, 55–58 (2015).
3. R. Sato Turtelli, Giap V. Duong, W. Nunes, R. Grössinger, and M. Knobel, "Magnetic properties of nanocrystalline $CoFe_2O_4$ synthesized by modified citrate-gel method," *J. Magn. Magn. Mater.*, **320**, e339–e342 (2008).
4. Dong-Hyun Kim, Se-Ho Lee, Kyoung-Nam Kim, Kwang-Mahn Kim, In-Bo Shim, and Yong-Keun Lee, "Temperature change of various ferrite particles with alternating magnetic field for hyperthermic application," *J. Magn. Magn. Mater.*, **293**, 320–327 (2005).
5. A.B. Shinde, "Structural and electrical properties of cobalt ferrite Nanoparticles," *Int. J. Innovative Technol. Exploring Eng.* (*IJITEE)*, **3**, 64–67 (2013).
6. R.M. Rosnan, Z. Othaman, R. Hussin, Ali A. Ati, Alireza Samavati, Shadab Dabagh, and Samad Zare, "Effects of Mg substitution on the structural and magnetic properties of $Co_{0.5}Ni_{0.5-x}Mg_xFe_2O_4$ nanoparticle ferrites," *Chin. Phys. B*, **25**, 047501–047507 (2016).
7. Jitendra Pal Singh, Hemanut Kumar, Ayush Singhal, Neelmanee Sarin, R.C. Srivastava, and Keun Hwa Chae, "Solubility limit, magnetic interaction and conduction mechanism in rare earth doped spinel ferrite," *Appl. Sci. Letter*, **2**, 3–11 (2016).
8. Vithal Vinayak, Pankaj P. Khirade, Shankar D. Birajdar, P.K. Gaikwad, N.D. Shinde, and K.M. Jadhav, "Low temperature synthesis of magnesium doped cobalt ferrite nanoparticles and their structural properties," *Int. Adv. Research J. Sci., Eng. Technol.*, **2**, 55–58 (2015).
9. Ulises A. Agú, Marcos I. Oliva, Sergio G. Marchetti, Angélica C. Heredia, Sandra G. Casuscelli, and Mónica E. Crivello, "Synthesis and characterization of a mixture of $CoFe_2O_4$ and $MgFe_2O_4$ from layered double hydroxides: Band gap energy and magnetic responses," *J. Magn. Magn. Mater.*, **369**, 1–11 (2014).
10. Noorhana Yahya1, Muhammad Kashif, Nadeem Nasir, Majid Niaz Akhtar, and Noorasikin Mohd, "Cobalt ferrite nanoparticles: An innovative approach for enhanced oil recovery application," *J. Nano Research*, **17**, 115–126 (2012).
11. D.R.S. Gangaswamy, M. Chaitanya Varma, S. Bharadwaj, K. SambasivaRao, K.H. Rao, "Comparison study of structural and magnetic properties of magnesium-substituted nickel–zinc ferrites synthesized by solid-state and sol–gel routes," *J. Superconductivity Novel Magnetism*, **28**, 3599–3606 (2015).
12. E. Wu, "POWD. An interactive program for powder diffraction data interpretation and indexing," *J. Appl. Crystallography*, **22**, 506–510 (1989)..
13. A.L. Patterson, "The scherrer formula for X-ray particle size determination," *Phys. Rev.*, **56**, 978–982 (1939).
14. Vikram S. Yadav, Devendra K. Sahu, Yashpal Singh, and D.C. Dhubkarya, "The effect of frequency and temperature on dielectric properties of pure poly vinylidene fluoride (PVDF) thin films, in: *Proc. Int. Multi Conference of Engineers and Computer Scientists*, **3 (**2010), p. 1–4.
15. Razia Nongjai, Shakeel Khan, K. Asokan, Hilal Ahmed, and Imran Khan, "Magnetic and electrical properties of In doped cobalt ferrite nanoparticles," *J. Appl. Phys.*, **112**, 084321-1-8 (2012).

16. J. Ross Mac Donald, “Impedance spectroscopy,” *Annals Biomedical Eng.*, 289–305 (1992).
17. S.K. Satpathy, N.K. Mohanty, A.K. Behera, S. Sen, Banarjee Behera, and P. Nayak, “Dielectric and electrical properties of $BiFeO_3$–$PbZrO_3$ composites,” *J. Electron. Mater.*, 1–10 (2015).
18. S.K. Satpathy, N.K. Mohanty, A.K. Behera, and Banarji Behera, “Dielectric and electrical properties of 0.5(BiGd0:05Fe0:95O_3)–0.5($PbZrO_3$) composite,” *Mater. Sci.-Poland*, **32**, 59–65 (2014).
19. J. Plocharski and W. Wieczoreck, “PEO based composite solid electrolyte containing NASICON,” *Sol. St. Ionics,* **28**, 979–982 (1988).
20. Ajay Kumar Behera, Nilaya K. Mohanty, Santosh K. Satpathy, Banarji Behera, Pratibindhya Nayak, “Investigation of complex impedance and modulus properties of Nd doped 0:5$BiFeO_3$–0:5$PbTiO_3$ multiferroic composites,” *Cent. Eur. J. Phys.*, **12**, 851–861 (2014).
21. Ibetombi Soibam, N. Nilima, and S. Phanjoubam, “Dielectric studies of double sintered lithium zinc nickel ferrite prepared by citrate precursor method,” *Am. J. Mater. Sci. Eng.*, **2**, 24–27 (2014).
22. F. Borsa, D.R. Torgeson, S.W. Martin, and H.K. Patel, “Relaxation and suctuations in glassy fast-ion conductors: Wide-frequency-range NMR and conductivity measurements,” *Phys. Rev. B*, **46**, 795–802 (1992).
23. D.C. Sinclair and A.R. West, “Impedance and modulus spectroscopy of semiconducting $BaTiO_3$ showing positive temperature coefficient of resistance,” *J. Appl. Phys.*, **66**, 3850–3856 (1989).
24. Soma Dutta, R.N.P. Choudhary, and P.K. Sinha, “Impedance spectroscopy studies on Fe^{3+} ion modified PLZT ceramics,” *Ceram. Int.*, **33**, 13–20 (2007).
25. A.K. Jonscher, “The ‘Universal’ dielectric response,” *Nature*, **267**, 673–679 (1977).
26. F.A. Najar, G.B. Vakil, and B. Want, “Structural, optical and dielectric studies of lithium sulphate monohydrate single crystals,” *Mater. Sci.-Poland*, **35(1)**, 18–31 (2017).
27. A.M. Mohammad, S.M. Ali Ridha, T.H. Mubarak, “Structural and magnetic properties of Mg–Co ferrite nanoparticles,” *Digest J. Nanomater. Biostruct.*, **13**, 615–623 (2018).